Investigation of flame surface density modeling for large eddy simulation of turbulent premixed flames by comparison with a prescribed reference solution

Denis Veynante

Investigation of flame surface density modeling for large eddy simulation of turbulent premixed flames by comparison with a prescribed reference solution

D. Veynante

Laboratoire EM2C, CNRS, Ecole CentraleSupélec, Université Paris-Saclay, 8 - 10 Rue Joliot Curie, 91192, Gif-sur-Yvette Cedex, France

---

Abstract

A framework is proposed to investigate the behavior of LES flame surface density models for simple academic cases, here the development of a statistically one-dimensional flame in an homogenous and isotropic turbulence, by comparison with a prescribed reference solution. First, a set of zero-dimensional equations is derived to reproduce a fractal flame surface evolving from an initially planar shape up to equilibrium. Then, a balance equation including a sub-grid scale contribution is solved to mimic the evolution of the overall resolved flame surface in an actual large eddy simulation.

Non-dynamic and dynamic versions of an algebraic sub-grid scale flame surface wrinkling factor model are investigated. The non-dynamic model overestimates the total flame surface in early stages of the flame development while under (respectively over) estimation of unresolved surfaces are partly compensated by larger (respectively lower) resolved surfaces. Moreover, model parameters strongly affect flame response times possibly compromising the prediction of combustion instabilities. Results are improved using a dynamic flame surface wrinkling factor model.

The generality of conclusions are limited by the enforcement of the reference solution but the proposed approach is well-suited to qualitative investigations of sub-grid scale models at negligible computational costs, to support direct numerical simulation studies or to help in analyzing LES results. It also suggests new possible closures for future developments.

Keywords: Turbulent premixed combustion, Flame surface density modeling, Large eddy simulation, Sub-grid scale models, Theoretical analysis

---

1. Introduction

The pioneering work of Kenneth Bray and coworkers [1–8] who introduced progress variable and assumed infinitely thin flame fronts to investigate the physics, evidencing counter-gradient transport, and model turbulent premixed combustion, i.e. developing the so-called BML formalism (Bray-Moss-Libby, or the Bi-Modal Limit following to the authors' modesty), was the foundation of numerous contributions regarding flamelet modeling. Among them, a class of models quantifies the flame surface, identified to a given level c^* of the progress variable. This approach splits the reaction rate into two contributions, the reaction rate per unit of flame area, modeled from laminar flame characteristics, and the flame surface density measuring the flame surface per unit volume, Σ^*, describing the flame / turbulence interaction and estimated from an algebraic expression or solving a balance

equation [8–16].[1]

Initially devised for Reynolds averaged Navier-Stokes (RANS) equations, the flame surface density concept was easily extended to large eddy simulation (LES), either using an algebraic expression or solving a balance equation [18–27].[2] Boger et al. [18] introduced a "generalized" flame surface density Σ integrating Σ^* over all the c-surfaces (see also [24]) and extended to LES the flame surface density algebraic expression devised by Bray et al. [8]. Some of the above models measure the flame surface in terms of wrinkling factor, Ξ, i.e. the ratio of the flame surface to its projection on a plane normal to the propagating direction, instead of flame surface density. Large eddy simulation gives the opportunity to take advantage of the known resolved flame wrinkles to infer the behavior of the unresolved ones, through similarity assumptions [28–30] or dynamically adjusting model parameters [29–42].

Numerous contributions have investigated flame surface density models and revisited closures for Reynolds averaged and large eddy simulations using direct numerical simulations (DNS) [see, for example, among many others, 15, 18, 23, 37, 43–53]. We propose here an alternative academical framework to investigate the behavior of flame surface density models in large eddy simulations. The idea is to prescribe exact and known solutions to the set

[1] The idea of solving a flame surface density balance equation was first proposed by Marble and Broadwell [17] for non-premixed combustion.

[2] Strictly speaking, Colin et al. [21] and Charlette et al. [23] works are related to the thickened flame model [TFLES, see also 27] but unresolved contributions to reaction rates are modeled using a flame surface wrinkling factor estimated from an equilibrium assumption in the flame surface density balance equation.

of equations for total, resolved and unresolved flame surfaces. Then, the influence of sub-grid scale models on resolved and total flame surfaces can be analyzed. Obviously, the generality of conclusions will be limited by the relevance of the exact solutions retained and the corresponding closures of the balance equations but *(i)* we feel this approach will contribute to draw some general trends and help to identify potential model drawbacks; *(ii)* some new closure schemes could emerge; *(iii)* many points can be investigated at negligible computational costs. In the case studied below, equations reduce to ordinary differential equations where quantities of interest evolve only with time.

In the following, we assume that the flame behaves as a fractal surface at all stages of its development, as suggested by various models and analysis [23, 28, 49, 54–65]. Once derived the balance equations describing the evolution of a statistically one-dimensional flame evolving in an homogenous and isotropic frozen turbulence (Section 2), exact closures are proposed to fit this requirement (Section 3) while the influence of two sub-grid scale models, a simple algebraic model and its dynamic version, on resolved and total flame surfaces, and then on the overall turbulent flame speed, as well as the unsteady flame response, are discussed in Section 4, including model parameter uncertainties. Conclusions and perpectives are drawn in Section 5.

2. Mathematical framework

2.1. Progress variable and flame surface density balance equations

Following Bray and Libby [1], a progress variable c, corresponding to a reduced mass fraction or temperature and increasing from $c = 0$ in pure fresh

gases to $c = 1$ in fully burnt products, is introduced under the assumptions of a single-step irreversible chemical reaction, adiabatic and isobaric combustion and unity species Lewis numbers. Its balance equation reads:

$$\frac{\partial c}{\partial t} + \mathbf{u} \cdot \nabla c = \frac{1}{\rho} \left[\nabla \cdot (\rho D \nabla c) + \dot{\omega}_c \right] = S_d \left| \nabla c \right| \tag{1}$$

where t is the time, ρ the density, $\mathbf{u}$ the velocity vector and $\dot{\omega}_c$ the progress variable reaction rate while the molecular diffusion flux is modeled following a Fick law with a diffusivity D. S_d is the c-surface displacement speed relatively to the flow and can be expressed in terms of a speed corrected of thermal expansion, S_d^0, according to $S_d = (\rho_0/\rho) S_d^0$ where ρ_0 is the fresh gas density. For a one-dimensional unstrained laminar flame, S_d^0 corresponds to the laminar flame speed S_L. A balance equation for $|\nabla c|$ is easily derived:

$$\frac{\partial \left| \nabla c \right|}{\partial t} + \nabla \cdot \left[\mathbf{u} \left| \nabla c \right| \right] = \left(\nabla \cdot \mathbf{u} - \mathbf{n}\mathbf{n} : \nabla \mathbf{u} \right) \left| \nabla c \right| - \nabla \cdot \left[S_d \mathbf{n} \left| \nabla c \right| \right] + S_d \nabla \cdot \mathbf{n} \left| \nabla c \right| \tag{2}$$

where $\mathbf{n} = -\nabla c / \left| \nabla c \right|$ is the unit vector normal the local c surface pointing towards fresh gases. RHS terms correspond to the strain rate induced by the flow field on the c-surface, the normal propagation term and a combined propagation / curvature term, respectively.

Applying an LES filter to Eq. (1) gives:

$$\frac{\partial \overline{\rho} \widetilde{c}}{\partial t} + \nabla \cdot \left(\overline{\rho \mathbf{u} c} \right) = \nabla \cdot \left(\overline{\rho D \nabla c} \right) + \overline{\dot{\omega}}_c = \overline{\rho S_d \left| \nabla c \right|} = \langle \rho S_d \rangle_s \Sigma_{gen} \tag{3}$$

where $\overline{Q}$ and $\widetilde{Q}$ denote the filtered Q quantity and the mass-weighted filtered quantity $\widetilde{Q} = \overline{\rho Q} / \overline{\rho}$, respectively, while $\Sigma_{gen} = \overline{|\nabla c|}$ is the generalized flame surface density and $\langle Q \rangle_s = \overline{Q \left| \nabla c \right|} / \Sigma_{gen}$ defines surface averaging [18, 24]. Filtering Eq. (2) provides a balance equation for the generalized flame surface

density Σ_{gen}[9, 12, 15, 18, 22, 24]:

$$\frac{\partial \Sigma_{gen}}{\partial t} + \nabla \cdot [\langle \mathbf{u} \rangle_s \Sigma_{gen}] = \langle \nabla \cdot \mathbf{u} - \mathbf{nn} : \nabla \mathbf{u} \rangle_s \Sigma_{gen} - \nabla \cdot [\langle S_d \mathbf{n} \rangle_s \Sigma_{gen}] + \langle S_d \nabla \cdot \mathbf{n} \rangle_s \Sigma_{gen} \tag{4}$$

Equations (2) and (4) are now integrated over a volume $\mathcal{V}$ containing all the flame surface, leading to:

$$\frac{dS_{tot}}{dt} = \langle \nabla \cdot \mathbf{u} - \mathbf{nn} : \nabla \mathbf{u} \rangle_{tot} S_{tot} + \langle S_d \nabla \cdot \mathbf{n} \rangle_{tot} S_{tot} \tag{5}$$

where, remembering that an LES filter is conservative,

$$S_{tot} = \int_{\mathcal{V}} \Sigma_{gen} \, d\mathcal{V} = \int_{\mathcal{V}} |\nabla c| \, d\mathcal{V} \tag{6}$$

measures the total flame surface and

$$\langle Q \rangle_{tot} S_{tot} = \int_{\mathcal{V}} \langle Q \rangle_s \Sigma_{gen} \, d\mathcal{V} = \int_{\mathcal{V}} Q \, |\nabla c| \, d\mathcal{V} \tag{7}$$

defines $\langle Q \rangle_{tot}$ the averaging of Q over all the flame surface. Note that Eq. (5) also holds for a planar flame in a periodic box, the configuration investigated in Section 4 below, but the divergence term does not vanish in general if the flame touches a boundary of the integration volume $\mathcal{V}$.

2.2. Resolved flame surface

To go further, we now assume that the resolved flame surface behaves relatively to resolved flow motions as the actual flame in the turbulent flow, replacing the laminar flame speed, S_L and thickness δ_L by a sub-grid scale turbulent flame speed S_T^0 and a thickness of the order of the filter size Δ. This assumption is usual to close thickened flame [21, 23, 27, 66] or F-TACLES

[67] models where the lost unresolved flame wrinkling is replaced by an increased resolved flame propagation speed. Equation (3) is then recast in the propagation form:

$$\frac{\partial \widetilde{c}}{\partial t} + \widetilde{\mathbf{u}} \cdot \nabla \widetilde{c} = \frac{1}{\overline{\rho}} \left[\nabla \cdot \left(\overline{\rho D \nabla c} \right) + \overline{\dot{\omega}}_c - \nabla \cdot \left(\overline{\rho \mathbf{u} c} - \overline{\rho} \widetilde{\mathbf{u}} \widetilde{c} \right) \right] = S_T \left| \nabla \widetilde{c} \right| \tag{8}$$

defining the displacement speed S_T of the resolved $\widetilde{c}$-surface relatively to the resolved flow, with $\rho_0 S_T^0 = \overline{\rho} S_T$. As this equation is formally similar to Eq. (1), one easily deduces from Eq. (2) that:

$$\frac{\partial \left| \nabla \widetilde{c} \right|}{\partial t} + \nabla \cdot \left[\widetilde{\mathbf{u}} \left| \nabla \widetilde{c} \right| \right] = \left(\nabla \cdot \widetilde{\mathbf{u}} - \widetilde{\mathbf{n}} \widetilde{\mathbf{n}} : \nabla \widetilde{\mathbf{u}} \right) \left| \nabla \widetilde{c} \right| - \nabla \cdot \left[S_T \widetilde{\mathbf{n}} \left| \nabla \widetilde{c} \right| \right] + S_T \nabla \cdot \widetilde{\mathbf{n}} \left| \nabla \widetilde{c} \right| \tag{9}$$

where $\widetilde{\mathbf{n}} = -\nabla \widetilde{c} / \left| \nabla \widetilde{c} \right|$ is the normal vector to the resolved $\widetilde{c}$-surface pointing towards fresh gases. Then,

$$\frac{dS_{res}}{dt} = \langle \nabla \cdot \widetilde{\mathbf{u}} - \widetilde{\mathbf{n}} \widetilde{\mathbf{n}} : \nabla \widetilde{\mathbf{u}} \rangle_{res} S_{res} + \langle S_T \nabla \cdot \widetilde{\mathbf{n}} \rangle_{res} S_{res} \tag{10}$$

where resolved flame surface and surface average are defined as:

$$S_{res} = \int_{\mathcal{V}} \left| \nabla \widetilde{c} \right| \, d\mathcal{V} \quad \text{and} \quad \langle Q \rangle_{res} S_{res} = \int_{\mathcal{V}} Q \left| \nabla \widetilde{c} \right| \, d\mathcal{V} \tag{11}$$

2.3. Mean flame surface wrinkling factors

Considering a statistically one-dimensional flame evolving in a turbulent flow field and assuming flame periodicity in directions normal to the mean propagation, equations (5) and (10) can be recast in terms of mean total, Ξ_{tot}, and resolved, Ξ_{res}, flame wrinkling factors:

$$\Xi_{tot} = \frac{S_{tot}}{S_0} \quad ; \quad \Xi_{res} = \frac{S_{res}}{S_0} \tag{12}$$

where S_0 is the flame surface projected on a plane normal to the propagation direction (i.e. the surface of this plane). As S_0 is constant in this case, Ξ_{tot}

and Ξ_{res} balance equations are formally similar to S_{tot} and S_{res} equations, respectively, and can be written:

$$\frac{1}{\Xi_{tot}}\frac{d\Xi_{tot}}{dt} = \langle a \rangle_{tot} + \langle S_d \nabla \cdot \mathbf{n} \rangle_{tot} \quad (13)$$

$$\frac{1}{\Xi_{res}}\frac{d\Xi_{res}}{dt} = \langle a \rangle_{res} + \langle S_T \nabla \cdot \widetilde{\mathbf{n}} \rangle_{res} \quad (14)$$

where strain rate terms are noted $\langle a \rangle_{tot}$ and $\langle a \rangle_{res}$ for compactness. The mean wrinkling factor of the sub-grid scale surface, Ξ_{sgs}, is defined as:

$$\Xi_{sgs} = \frac{S_{tot}}{S_{res}} \quad \text{or} \quad \Xi_{tot} = \Xi_{sgs}\Xi_{res} \quad (15)$$

A balance equation for Ξ_{sgs} is then obtained subtracting Eq. (14) from Eq. (13):

$$\frac{1}{\Xi_{sgs}}\frac{d\Xi_{sgs}}{dt} = \underbrace{\langle a \rangle_{tot} - \langle a \rangle_{res}}_{\langle a \rangle_{sgs}} + \underbrace{\langle S_d \nabla \cdot \mathbf{n} \rangle_{tot} - \langle S_T \nabla \cdot \widetilde{\mathbf{n}} \rangle_{res}}_{\langle S_d \nabla \cdot \mathbf{n} \rangle_{sgs}} \quad (16)$$

Equations (13), (14) and (16) are exact for a statistically one-dimensional turbulent premixed flame but unclosed. In practical large eddy simulations, a model is required for Ξ_{sgs}, either an algebraic expression [21, 23, 68, 69] or solving a balance equation [19, 22, 25], while Ξ_{res} corresponds to resolved flame wrinkling and $\Xi_{tot} = \Xi_{sgs}\Xi_{res}$. In the following, Eq. (14), combined with adapted closures and a sub-grid scale model for Ξ_{sgs}, will be solved to mimic an actual LES, Eq. (13) providing the reference solution.

3. Closure schemes

3.1. Definition of a model problem

Equations (13 - 14) are now closed requiring solutions given by known expressions. We assume that the flame behave as a fractal surface at all

stages of its development [23, 28, 49, 54–65]:

$$\Xi_{tot} = \left(\frac{l_t}{\delta_c}\right)^{\beta} \quad ; \quad \Xi_{res} = \left(\frac{l_t}{\delta_\Delta}\right)^{\beta} \quad ; \quad \Xi_{sgs} = \left(\frac{\delta_\Delta}{\delta_c}\right)^{\beta} \tag{17}$$

where l_t is the turbulence integral length scale, identified to the outer cut-off scale of the fractal surface, δ_c and δ_Δ the inner cut-off scales of the total and resolved surfaces, respectively, and $D = 2 + \beta$, the fractal dimension evolving with time. The inner cut-off scales of the flame surface, δ_c, and of the resolved flame surface, δ_Δ, are expected to be of the order of the laminar flame thickness δ_L and the filter size Δ, respectively, but could differ. Gulder and Smallwood [70] suggested a dependence of δ_c with the Karlovitz number Ka ($\delta_c \propto \delta_L Ka^{-1/3}$), while Colin et al. [21] noted that resolved flow motions smaller than five times the thickness of the resolved flame have a reduced contribution to its wrinkling. However, these points are not addressed here and left for further investigations.

Equations (13) and (14) become:

$$\ln\left(\frac{l_t}{\delta_c}\right)\frac{d\beta_{tot}}{dt} = \langle a\rangle_{tot} + \langle S_d \nabla\cdot\mathbf{n}\rangle_{tot} \tag{18}$$

$$\ln\left(\frac{l_t}{\delta_\Delta}\right)\frac{d\beta_{res}}{dt} = \langle a\rangle_{res} + \langle S_T \nabla\cdot\widetilde{\mathbf{n}}\rangle_{res} \tag{19}$$

and are expected to provide the same solution $\beta = \beta_{tot} = \beta_{res}$. We now look for closures of strain rate and curvature terms achieving this goal.

3.2. Strain rate term closure

Assuming that strain rate terms $\langle a\rangle_{tot}$ and $\langle a\rangle_{res}$ can be modeled independently of propagation / curvature terms $\langle S_d \nabla\cdot\mathbf{n}\rangle_{tot}$ and $\langle S_T \nabla\cdot\widetilde{\mathbf{n}}\rangle_{res}$ and comparing equations (18) and (19) suggest the rather unusual scaling:

$$\frac{\langle a\rangle_{tot}}{\ln\left(l_t/\delta_c\right)} = \frac{\langle a\rangle_{res}}{\ln\left(l_t/\delta_\Delta\right)} \tag{20}$$

Following the procedure proposed by Charlette et al. [23], the strain rate due to turbulent motions in the range of the flame inner cut-off scale δ_c and the integral length scale l_t is given by (see Eq. (A.4) and its derivation in AppendixA):

$$\langle a \rangle_{tot} = \frac{3}{\sqrt{55}} Ka \frac{S_L}{\delta_L} \left[\exp\left(-\frac{3}{2} C_k \frac{\pi^{4/3}}{Re_t} \right) - \exp\left(-\frac{3}{2} C_k \frac{\pi^{4/3}}{Re_t} \left(\frac{l_t}{\delta_c} \right)^{4/3} \right) \right]^{1/2} \tag{21}$$

where the turbulence Reynolds number and the Karlovitz number are $Re_t = u' l_t / \nu$ and $Ka = (u'/S_L)^{3/2} (l_t/\delta_L)^{-1/2}$, respectively, u' being the velocity fluctuation related to integral length scale l_t, S_L the laminar flame speed and ν the kinematic viscosity [27]. $C_k \approx 1.5$ is the universal Kolmogorov constant.

Comparing Eqs. (20) and (21) suggests to model the strain rate acting on the resolved flame surface, $\langle a \rangle_{res}$ as:

$$\begin{aligned} \langle a \rangle_{res,1} &= \frac{3}{\sqrt{55}} Ka \frac{S_L}{\delta_L} \left[\exp\left(-\frac{3}{2} C_k \frac{\pi^{4/3}}{Re_t} \right) - \exp\left(-\frac{3}{2} C_k \frac{\pi^{4/3}}{Re_t} \left(\frac{l_t}{\delta_c} \right)^{4/3} \right) \right]^{1/2} \\ &\times \frac{\ln\left(l_t/\delta_\Delta\right)}{\ln\left(l_t/\delta_c\right)} \end{aligned} \tag{22}$$

while applying Eq. (21) to the cut-off scale δ_Δ gives:

$$\langle a \rangle_{res,2} = \frac{3}{\sqrt{55}} Ka \frac{S_L}{\delta_L} \left[\exp\left(-\frac{3}{2} C_k \frac{\pi^{4/3}}{Re_t} \right) - \exp\left(-\frac{3}{2} C_k \frac{\pi^{4/3}}{Re_t} \left(\frac{l_t}{\delta_\Delta} \right)^{4/3} \right) \right]^{1/2} \tag{23}$$

Figure 1 compares $\langle a \rangle_{res,1}$ and $\langle a \rangle_{res,2}$ as predicted by Eqs. (22) and (23), respectively, for $Re_t = 34$ and $l_t/\delta_c = 20$, retained for tests below (see Table 2), as function of δ_Δ/l_t. Values are identical for $\delta_\Delta = \delta_c$ and $\delta_\Delta = l_t$ by construction, but slightly differ elsewhere. However, the scaling in Eq. (20)

is acceptable, especially considering the strong assumptions underlying the derivation of Eq. (21) [see AppendixA and Refs 21, 23, 43]. Note that the discrepancies between $\langle a \rangle_{res,1}$ and $\langle a \rangle_{res,2}$ decrease when increasing Reynolds number Re_t (or u'/S_L) for a constant ratio l_t/δ_c (not shown for brevity). In the following, we will retain the simplified expressions, sufficient for our objectives:

$$\langle a \rangle_{tot} = \alpha K a \frac{S_L}{\delta_L} \ln\left(\frac{l_t}{\delta_c}\right) \quad \text{and} \quad \langle a \rangle_{res} = \alpha K a \frac{S_L}{\delta_L} \ln\left(\frac{l_t}{\delta_\Delta}\right) \tag{24}$$

where α is a model parameter. According to Eq. (16), $\langle a \rangle_{sgs}$ is modeled as:

$$\langle a \rangle_{sgs} = \langle a \rangle_{tot} - \langle a \rangle_{res} = \alpha K a \frac{S_L}{\delta_L} \ln\left(\frac{\delta_\Delta}{\delta_c}\right) \tag{25}$$

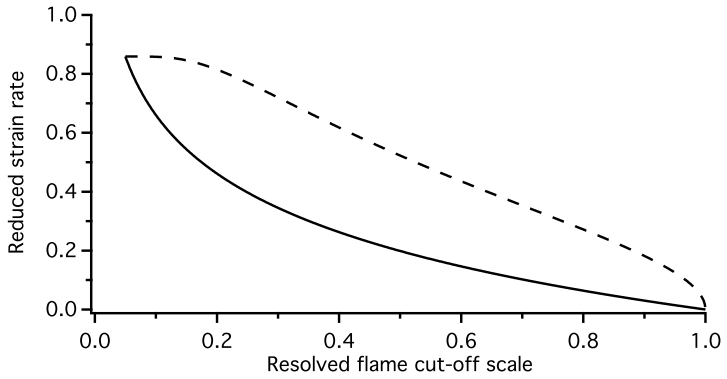

Figure 1: Comparison of strain rates $\langle a \rangle_{res,1}$ (present model, Eq. 22, continuous line) and $\langle a \rangle_{res,2}$ (Charlette et al. [23] model, Eq. 23, dashed line) plotted as a function of the ratio δ_Δ/l_t for $Re_t = 34$ and $l_t/\delta_c = 20$ (see Table 2). Displayed values are divided by the coefficient $(3/\sqrt{55})Ka(S_L/\delta_L)$.

3.3. Combined propagation / curvature term closure

3.3.1. Total flame surface wrinkling factor equation ($\langle S_d \nabla \cdot \mathbf{n} \rangle_{tot}$)

Following Peters [59, 71] the displacement speed S_d defined by Eq. (1) is decomposed into three components:

$$S_d = \underbrace{\frac{\dot{\omega}_c}{\rho \left| \nabla c \right|}}_{S_r} + \underbrace{\frac{\mathbf{n} \cdot \nabla \left(\rho D \mathbf{n} \cdot \nabla c \right)}{\rho \left| \nabla c \right|}}_{S_n} - \underbrace{D \nabla \cdot \mathbf{n}}_{S_t} \tag{26}$$

due to reaction rate, normal diffusion and tangential diffusion, respectively. Direct numerical simulation data suggest that, for statistically planar flames, $S_r + S_n$, which is of the order of $(\rho_0/\rho) S_L$, where ρ_0 is the fresh gas density, is only weakly correlated to the curvature $\nabla \cdot \mathbf{n}$ [see, for example, 47, 59, 71], at least for unity Lewis number flames, while the mean curvature is close to 0 [see, among many others, 47, 72]. Then:

$$\langle S_d \nabla \cdot \mathbf{n} \rangle_{tot} \approx - \langle D \left(\nabla \cdot \mathbf{n} \right)^2 \rangle_{tot} \tag{27}$$

The variance of the curvature is expected to scale with the square of the inverse of the flame surface wrinkling length scale L_y. Bray et al. [8] correlated L_y to the turbulence integral length scale l_t and the ratio of the turbulent intensity u' and the laminar flame speed S_L:

$$L_y = C_l l_t \left(\frac{S_L}{u'} \right)^n \tag{28}$$

where C_l and n are model parameters, while Colin et al. [21] and Charlette et al. [23] proposed:[3]

$$L_y = C_l \frac{l_t}{\Xi_{tot} - 1} \tag{29}$$

[3]Written for the unresolved contribution, in terms of filter size Δ and sub-grid scale wrinkling factor Ξ_{sgs}, in references [21, 23].

These expressions are close as $1 + (u'/S_L)^n$, with n of order unity, is a good estimate of the wrinkling factor Ξ_{tot} in the flamelet regime. However, they are not adapted to recover a fractal solution (17) for Eq. (13). In this view, considering two limiting cases:

- For a planar laminar flame: $\Xi_{tot} = 1$, $\beta_{tot} = 1$ and $L_y = +\infty$ (unwrinkled flame surface).
- When the flame occupies all the available volume (space-filling limit with a fractal dimension $D = 3$), $\Xi_{tot} = l_t/\delta_c$, $\beta_{tot} = 1$ and $L_y \approx \delta_c$.

suggests the simple scaling $L_y \propto \delta_c/\beta_{tot}^n$, where exponent n is a model parameter. Assuming $D \approx S_L\delta_L$, $\delta_c \approx \delta_L$ and keeping the factor $\ln(l_t/\delta_c)$ found in the LHS of Eq. (18) and introduced in the modeling of $\langle a \rangle_{tot}$ (Eq. 24), the curvature term is then modeled as:

$$\langle S_d \nabla \cdot \mathbf{n} \rangle_{tot} \approx -\gamma D \left(\frac{\beta_{tot}^n}{\delta_c} \right)^2 \ln \left(\frac{l_t}{\delta_c} \right) \approx -\gamma \frac{S_L}{\delta_L} \beta_{tot}^{2n} \ln \left(\frac{l_t}{\delta_L} \right) \tag{30}$$

where γ is a model parameter. Setting $n = 1/2$ introduces the logarithm of the flame wrinkling factor $\Xi_{tot} = (l_t/\delta_L)^{\beta_{tot}}$:

$$\langle S_d \nabla \cdot \mathbf{n} \rangle_{tot} \approx -\gamma \frac{S_L}{\delta_L} \beta_{tot} \ln \left(\frac{l_t}{\delta_L} \right) = -\gamma \frac{S_L}{\delta_L} \ln \left(\Xi_{tot} \right) \tag{31}$$

This expression scales L_y as $L_y \propto \delta_c [\ln(\Xi_{tot})]^{-1/2}$, referring to the inner cut-off scale δ_c, while Eqs (28-29) correspond to $L_y \propto l_t (\Xi_{tot} - 1)^{-1}$, using the outer cut-off scale l_t. To analyse these discrepancies is left for future investigations.

3.3.2. Resolved flame surface wrinkling factor equation ($\langle S_T \nabla \cdot \widetilde{\mathbf{n}} \rangle_{res}$)

Assuming that the resolved flame surface behaves as a laminar flame of thickness $\Delta \approx \delta_\Delta$ propagating at the flame speed $\Xi_{sgs} S_L$, Eq. (31) suggests:

$$\langle S_T \nabla \cdot \widetilde{\mathbf{n}} \rangle_{res} \approx -\gamma \frac{\Xi_{sgs} S_L}{\Delta} \ln \left(\Xi_{res} \right) \tag{32}$$

scaling the resolved flame wrinkling length scale as $L_y^\Delta \propto \Delta[\ln(\Xi_{res})]^{-1/2}$. However, combining this expression with Eqs (24) and (31) would close Eqs (18-19) as:

$$\frac{d\beta_{tot}}{dt^+} = \alpha Ka - \gamma\beta_{tot} \quad ; \quad \frac{d\beta_{res}}{dt^+} = \alpha Ka - \gamma\frac{\Xi_{sgs}}{\Delta/\delta_L}\beta_{res} \tag{33}$$

giving different β_{tot} and β_{res} values excepted when $\Xi_{sgs} = \Delta/\delta_L$, i.e. $\beta_{sgs} = 1$, missing the objective of a fractal solution in the range $[\delta_c, l_t]$, with $\beta_{tot} = \beta_{res} = \beta_{sgs}$. Keeping the idea of a resolved flame speed equals to $\Xi_{sgs}S_L$ and a similar form of the closure scheme suggest to modify the modeling of the resolved flame surface wrinkling length scale, L_y^Δ:

- $L_y^\Delta \propto \Xi_{sgs}\delta_c[\ln(\Xi_{res})]^{-1/2} \approx \Xi_{sgs}\delta_L[\ln(\Xi_{res})]^{-1/2}$ (i.e. replacing Δ by $\Xi_{sgs}\delta_L$ in Eq. 32) would fit the goal but fully decouples Eqs (33), that is not physical: increasing the sub-grid scale wrinkling factor and the sub-grid scale turbulent flame speed is expected to reduce the sensitivity of the resolved flame to resolved turbulent motions.

- $L_y^\Delta \propto \delta_c(\delta_\Delta/\delta_c)^{\beta_{res}}[\ln(\Xi_{res})]^{-1/2} \approx \delta_L(\Delta/\delta_L)^{\beta_{res}}[\ln(\Xi_{res})]^{-1/2}$ (i.e. replacing Δ by $\delta_L(\Delta/\delta_L)^{\beta_{res}}$ in Eq. 32) also fits the goal as the fractal solution corresponds to $\beta_{sgs} = \beta_{res}$ and $\Xi_{sgs} = (\delta_\Delta/\delta_c)^{\beta_{sgs}} \approx (\Delta/\delta_L)^{\beta_{res}}$. Equations (33) then predict as expected $\beta_{tot} = \beta_{res}$. Note that, when flame wrinkles are fully resolved (DNS limit), $\delta_\Delta/\delta_c \to 1$, $\Xi_{res} \to \Xi_{tot}$ and $L_y^\Delta \to L_y$, as expected. In the following, we then adopt the simple ad hoc closure:

$$\langle S_T\nabla\cdot\widetilde{\mathbf{n}}\rangle_{res} \approx -\gamma\frac{\Xi_{sgs}S_L}{(\delta_\Delta/\delta_c)^{\beta_{res}}\,\delta_L}\ln(\Xi_{res}) \approx -\gamma\frac{\Xi_{sgs}S_L}{(\Delta/\delta_L)^{\beta_{res}}\,\delta_L}\ln(\Xi_{res}) \tag{34}$$

Equation (34) is a first step and undoubtedly the weakest point of the proposed derivation, requiring future investigations.

3.4. Summary and comments

The closed balance equations are then:

$$\frac{1}{\Xi_{tot}}\frac{d\Xi_{tot}}{dt^+} = \alpha Ka \ln\left(\frac{l_t}{\delta_c}\right) - \gamma \ln\left(\Xi_{tot}\right) \quad (35)$$

$$\frac{1}{\Xi_{res}}\frac{d\Xi_{res}}{dt^+} = \alpha Ka \ln\left(\frac{l_t}{\delta_\Delta}\right) - \gamma \frac{\Xi_{sgs}}{\left(\delta_\Delta/\delta_c\right)^{\beta_{res}}} \ln\left(\Xi_{res}\right) \quad (36)$$

or, in term of fractal dimension:

$$\frac{d\beta_{tot}}{dt^+} = \alpha Ka - \gamma\beta_{tot} \quad (37)$$

$$\frac{d\beta_{res}}{dt^+} = \alpha Ka - \gamma \frac{\Xi_{sgs}}{\left(\delta_\Delta/\delta_c\right)^{\beta_{res}}}\beta_{res} \quad (38)$$

introducing the reduced time $t^+ = t/\tau_f$, where $\tau_f = \delta_L/S_L$ is a flame time scale. The balance equation (16) for the sub-grid scale flame wrinkling factor Ξ_{sgs} is then implicitly closed as:

$$\begin{aligned}\frac{1}{\Xi_{sgs}}\frac{d\Xi_{sgs}}{dt^+} &= \alpha Ka \ln\left(\frac{\delta_\Delta}{\delta_c}\right) - \gamma \ln\left(\Xi_{sgs}\right) \\ &+ \gamma\left[\frac{\Xi_{sgs}}{\left(\delta_\Delta/\delta_c\right)^{\beta_{res}}} - 1\right]\ln\left(\Xi_{res}\right)\end{aligned} \quad (39)$$

where the last term models the influence of resolved scales on sub-grid scale wrinkles.

Considering an initially planar one-dimensional flame (i.e. $\Xi_{tot}(t^+ = 0) = 1$ and $\beta_{tot}(t^+ = 0) = 0$) evolving in a frozen homogeneous and isotropic turbulence, the analytical solution of Eq. (37) is:

$$\beta_{tot} = \frac{\alpha}{\gamma} Ka \left[1 - \exp\left(-\gamma t^+\right)\right] \quad (40)$$

corresponding to a fractal dimension $D = 2 + \beta_{tot} = 2 + \alpha Ka/\gamma$ when the turbulence / flame surface wrinkling equilibrium is reached ($t^+ \rightarrow +\infty$). This value is compared to others found in the literature in Table 1 and Fig. 2. Excepted the pioneering work by Gouldin [54] who proposed a value of D in the range 2.32 - 2.4, we limit this comparison to expressions written in terms of Karlovitz numbers. Lindstedt and Vaos [73] among others retained $D = 7/3$ while North and Santavicca [57] introduced a dependence of the velocity ratio u'/S_L and Giacomazzi et al. [60] a function of the turbulence Reynolds number. Expression $D = 2 + \beta = 2 + \alpha Ka/\gamma$ does not predict the expected saturation of the fractal dimension with increasing Karlovitz numbers but is sufficient as a first step in the flamelet regime. To predict this bending requires to modify strain rate and/or curvature terms in the flame surface wrinkling balance equation, left for future works. However, according to Fig. 2, $\alpha/\gamma = 3/4$ seems acceptable, corresponding to a line very close to the slope of the Chakraborty and Klein [45] expression in $Ka = 0$ (slope $4/(3\sqrt{\pi}) \approx 0.752$).

A last comment concerns the realizability of Eqs (36) and (38): a steady state regime can be reached only when β_{res} and $\Xi_{res} = (l_t/\delta_\Delta)^{\beta_{res}}$ can increase up to values making the second RHS term of the equations larger than or, at least, equal to the first one. In the particular case of a constant modeled wrinkling factor Ξ_{sgs}, this term increases with β_{res} up to reach $(\delta_\Delta/\delta_c)^{\beta_{res}} = \exp(1)$ and then decreases. Accordingly, the realizability condition is:

$$\gamma \Xi_{sgs} \geq \alpha Ka \exp(1) \ln\left(\frac{\delta_\Delta}{\delta_c}\right) \tag{41}$$

Table 1: Fractal dimension as a function of the Karlovitz number Ka.

Model	Fractal dimension D
Gouldin [54]	2.32 - 2.4
Chakraborty and Klein [45]	$2 + \frac{1}{3}\mathrm{erf}\,(2Ka)$
Keppeler et al. [65]	$\frac{8/3Ka + 2C_D}{Ka + C_D}$; $C_D = 0.03$
Present	$2 + \frac{\alpha}{\gamma}Ka$

4. Investigation of a statistically one-dimensional turbulent premixed flame

4.1. Introduction

We now consider a statistically one-dimensional premixed flame evolving in an homogeneous and isotropic frozen turbulence from an initially planar configuration ($\Xi_{tot} = \Xi_{res} = \Xi_{sgs} = 1$). Periodic boundary conditions are assumed in the directions normal to the mean propagation. The flame surface is progressively wrinkled by turbulent motions until an equilibrium state according to the exact reference solution given by Eq. (40). This simplified ideal case can be viewed as the development of a flame element from is anchoring location or following ignition. For example, a jet or swirling flame can be considered as laminar in the vicinity of the injector lips and is progres-

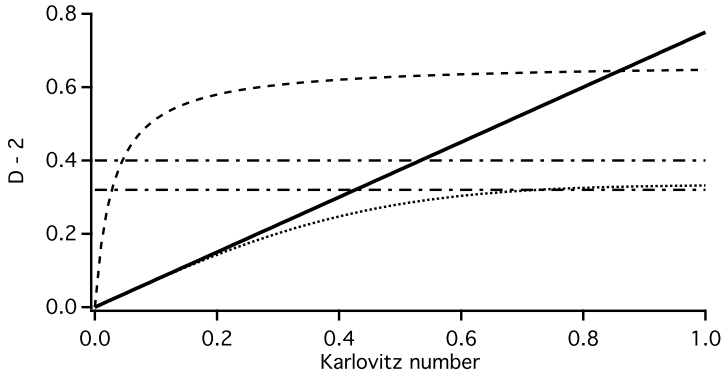

Figure 2: Model parameter $\beta = D - 2$ where D is the surface fractal dimension plotted as a function of the Karlovitz number Ka according to the expressions summarized in Table 1: dotted-dashed lines: range proposed by Gouldin [54]; dashed line: Keppeler et al. [65]; dotted line: Chakraborty and Klein [45]; line: present model with $\alpha/\gamma = 3/4$.

sively wrinkled by turbulent motions when convected downstream [see, for example, 37, 38]. A flame kernel developing in a turbulent field is laminar at early stages following ignition and is progressively wrinkled by ambiant turbulent motions [35, 74]. In these transient situations, turbulence and flame wrinkles have not reached equilibrium yet, an assumption underlying the derivation of algebraic models, motivating Richard et al. [25] to implement a flame surface density balance equation to predict combustion in internal combustion engines.[4]

In large eddy simulations, a model is set for the unresolved flame surface wrinkling, Ξ_{sgs}, while resolved scales are predicted by simulations. The cor-

[4]Note that the approach proposed here is close to the 0D formalism developed by Richard and Veynante [75] for internal combustion engines, considering an initially spherical flame surface progressively wrinkled by turbulent motions.

responding flame surface wrinkling factor Ξ_{res} is found here solving Eq. (36) with a simple explicit scheme implemented in Igor Pro software by WaveMetrics, running on a laptop. The objective is now to evaluate the impact of the Ξ_{sgs} model on the resolved (Ξ_{res}) and total ($\Xi_{tot} = \Xi_{sgs}\Xi_{res}$) flame surface wrinkling factors.

Chosen parameters are summarized in Table 2. As a flamelet regime is assumed, the Karlovitz number should be lower than unity. Arbitrarily setting this Karlovitz number to $Ka = 0.5$, as well as $\alpha = 3$, $\gamma = 4$ and $l_t/\delta_L = 20$, leads to the fractal dimension $D = 2.375$, in the range proposed by Gouldin [54], $u'/S_l \approx 1.7$, $Re_t = (u'l_t)/(S_L\delta_L) \approx 34$ and Damköhler number $Da \approx 12$. The exact equilibrium value of the total wrinkling factor is then $\Xi_{tot}^{eq} = (l_t/\delta_L)^{D-2} \approx 3.1$, identifying δ_c to the flame thickness δ_L. Simulations are displayed for $\delta_\Delta/\delta_L = 4$ ($l_t/\delta_L = 5$).

Table 2: Simulation parameters

Ka	D	l_t/δ_L	u'/S_L	Re_t	Da	α	γ	δ_Δ/δ_L
0.5	2.375	20.	1.7	34	12	3.	4.	4.

4.2. Constant sub-grid scale wrinkling factor

The sub-grid scale wrinkling factor Ξ_{sgs} is modeled as:

$$\Xi_{sgs} = \left(\frac{\delta_\Delta}{\delta_{c,m}}\right)^{\beta_m} \tag{42}$$

where the inner cut-off scale $\delta_{c,m}$ and the fractal dimension $D = 2 + \beta_m$ are prescribed by the user while the outer cut-off scale, δ_Δ, identified to the filter

size, is implicitly assumed to be known. Equation (42) corresponds to the "saturated form" of the Charlette et al. [23] expression, often observed in practice [37].

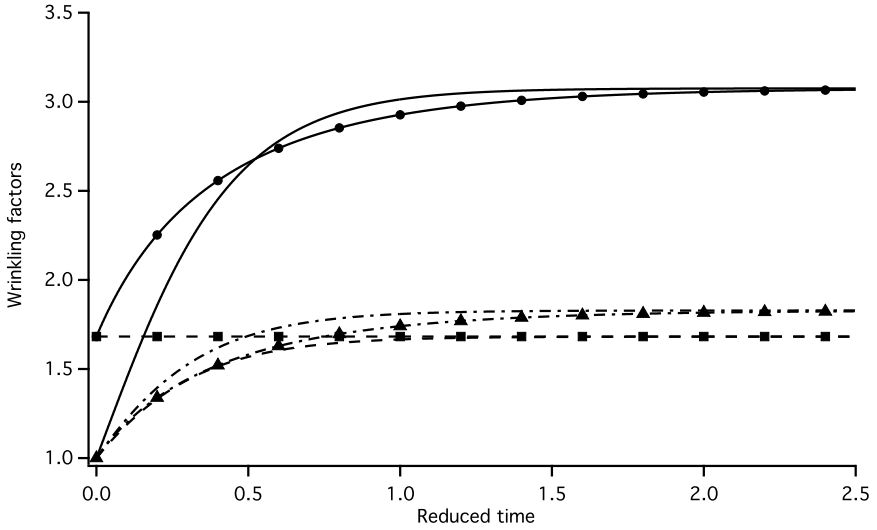

Figure 3: Evolution of the total (Ξ_{tot}, continuous line), resolved (Ξ_{res}, dotted-dashed line) and sub-grid scale (Ξ_{sgs}, dashed line) surface wrinkling factors as a function of the reduced time $t^+ = t/\tau_f$. Without markers: exact fractal reference solution; with markers: solution given by Eq. (36) combined with model (42) where $\beta_m = 0.375$ and $\delta_{c,m} = \delta_c$. See Table 2 for simulation parameters.

Figure 3 displays the evolution of exact and predicted total, resolved and sub-grid scale wrinkling factors with time when setting the inner cut-off scale to its exact value ($\delta_{c,m} = \delta_c = \delta_L$) and the model parameter to its exact equilibrium value ($\beta_m = 0.375$) with $\delta_\Delta = 4\delta_L$. The overestimation of the sub-grid scale flame surface wrinkling induces on overestimation of the total flame surface at early stages of the flame development, as already observed when comparing non-dynamic and dynamic flame wrinkling models [35, 37,

38]. This overestimation is partly compensated by a slight underestimation of the resolved flame surface. The response time of the flame is also affected and the equilibrium state is reached later. However, as the model parameters are set to their exact equilibrium values, this final stage is exactly recovered.

When β_m is set to $\beta_m = 0.5$, larger than the expected equilibrium value but corresponding to the value recommended by Charlette et al. [23], keeping the correct inner cut-off scale δ_c, the resolved flame surface is underestimated but cannot compensate the overestimation of the sub-grid scale wrinkling factor, leading to an slight overestimation of the total flame surface and then of the turbulent flame speed $S_T = \Xi_{tot} S_L$ (about 1 %) when equilibrium is reached (Fig. 4). Of course, this overestimation increases with the length scale ratio δ_Δ/δ_L (about 5.4 % for $\delta_\Delta/\delta_L = 6$). On the other hand, a too small $\beta_m = 0.26$ value leads to an overestimation of the resolved flame surface overcompensating the decreased unresolved flame surface (Fig. 5). The total flame surface is still larger than expected by about 23 % at the equilibrium, while the flame response is slower. Note that $\beta_m = 0.26$ is close of the minimum value imposed by the realizability condition (41) giving here $\beta_m \geq 0.25$. Similar results are found when varying $\delta_{c,m}$ but not detailed here for brevity.

Figure 6 displays equilibrium values of total, resolved and unresolved wrinkling factors reduced by their exact values varying model parameters β_m (left) and $\delta_{c,m}$ (right). In both cases, the value of the equilibrium turbulent flame speed (or Ξ_{tot}) is overestimated when the modeled sub-grid scale wrinkling factor Ξ_{sgs} is lower than the exact equilibrium value (i.e. $\beta_m < 0.375$ or $\delta_{c,m} > \delta_c$). Low values of Ξ_{sgs} are overcompensated by large resolved

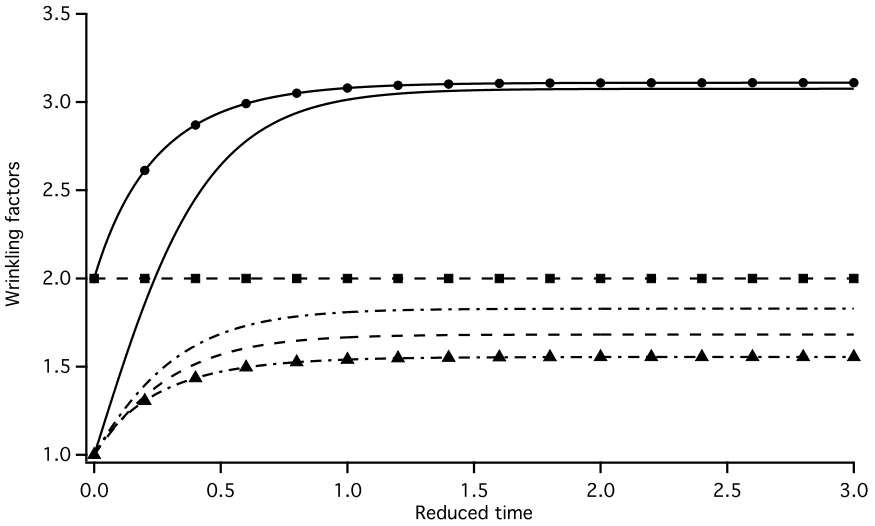

Figure 4: Evolution of the total (Ξ_{tot}, continuous line), resolved (Ξ_{res}, dotted-dashed line) and sub-grid scale (Ξ_{sgs}, dashed line) surface wrinkling factors as a function of the reduced time $t^+ = t/\tau_f$. Without markers: exact fractal reference solution; with markers: solution given by Eq. (36) combined with model (42) where $\beta_m = 0.5$ and $\delta_{c,m} = \delta_c$. See Table 2 for simulation parameters.

flame surfaces (see Fig. 5). On the other hand, large modeled Ξ_{sgs} values ($\beta_m > 0.375$ or $\delta_{c,m} < \delta_c$) are rather well compensated by low resolved flame surfaces. However, the error on the turbulent flame speed remains acceptable (below 10 %) in a large range of parameters ($0.29 \leq \beta_m \leq 0.5$ when $\delta_{c,m} = \delta_c$ and $0.5\delta_c \leq \delta_{c,m} \leq 1.4\delta_c$ with $\beta_m = 0.375$, the realizability condition (41) prescribing $\delta_{c,m} \leq 1.59\delta_c$ in this last case). As expected, this error increases (decreases) with the ratio δ_Δ/δ_L (not shown).

The response time of the flame wrinkling, τ_w, is evaluated by fitting a function $A + B\exp(-t/\tau_w)$ on the time evolution of the total flame surface wrinkling factor Ξ_{tot}. This time is reduced by the response time of the exact

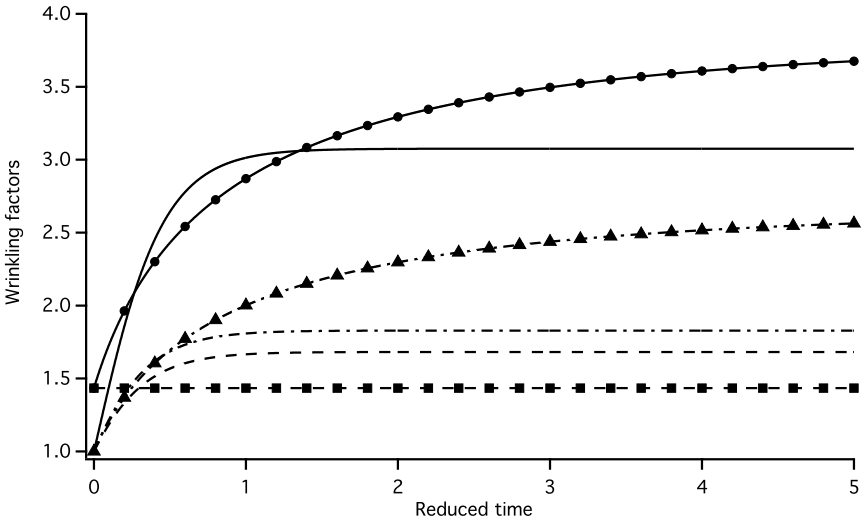

Figure 5: Evolution of the total (Ξ_{tot}, continuous line), resolved (Ξ_{res}, dotted-dashed line) and sub-grid scale (Ξ_{sgs}, dashed line) surface wrinkling factors as a function of the reduced time $t^+ = t/\tau_f$. Without markers: exact fractal reference solution; with markers: solution given by Eq. (36) combined with model (42) where $\beta_m = 0.26$ and $\delta_{c,m} = \delta_c$. See Table 2 for simulation parameters.

reference solution and displayed in Fig. 7 when varying β_m or $\delta_{c,m}$. Model parameters affect clearly the response time that increases when reducing the sub-grid scale wrinkling factor (i.e. decreasing β_m or increasing $\delta_{c,m}$), up to a factor larger than three when $\delta_{c,m} \geq 1.45\delta_c$ or $\beta_m \leq 0.27$, close to the realizability limits given by Eq. (41). Even setting the exact inner cut-off scale ($\delta_{c,m} = \delta_c$) and equilibrium fractal dimension ($\beta_m = 0.375$) affects the flame response time by a factor about 1.5. This finding is not surprising as the constant wrinkling factor model cannot reproduce the exact flame development but suggests that the prediction of possible combustion instabilities could be significantly affected, as the flame response time to flow

perturbations in a key ingredient in their mechanisms.

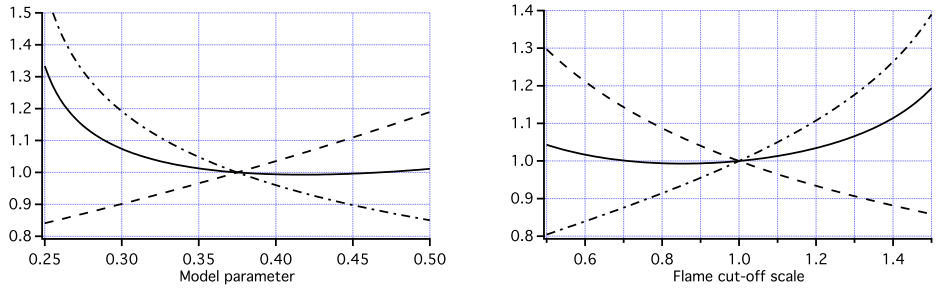

Figure 6: Evolution of equilibrium values of the total (Ξ_{tot}, continuous line), resolved (Ξ_{res}, dotted-dashed line) and sub-grid scale (Ξ_{sgs}, dashed line) surface wrinkling factors reduced by their exact values as a function of the model parameter β_m (left, $\delta_{c,m} = \delta_c$) and the flame cut-off length scale $\delta_{c,m}/\delta_c$ (right, $\beta_m = 0.375$).

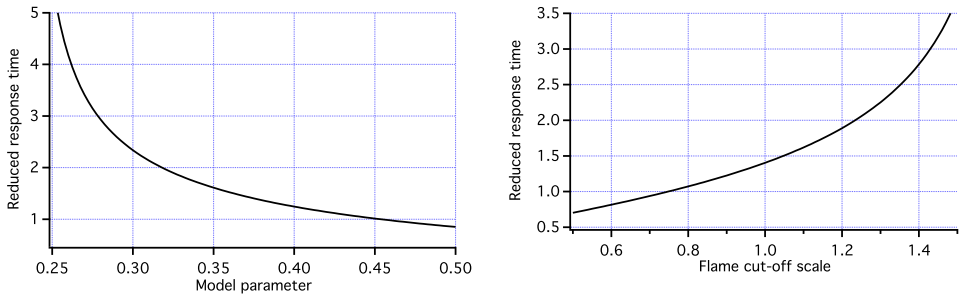

Figure 7: Evolution of the flame response time τ_w reduced by its exact value as a function of the model parameter β_m (left, $\delta_{c,m} = \delta_c$) and the flame cut-off length scale $\delta_{c,m}/\delta_c$ (right, $\beta_m = 0.375$).

4.3. Dynamic sub-grid scale wrinkling factor

A dynamic sub-grid scale wrinkling factor model [34–42] where $\Xi_{res} = (\delta_\Delta/\delta_c)^{\beta_{res}}$ using the model parameter β_{res} extracted from resolved scales

(assuming that the actual LES test filtering operating provides the correct β_{res} value), would give by construction the exact solution as long as the inner cut-off length scale δ_c is correctly set because Eqs (37) and (38) become identical. Moreover, when $\Xi_{sgs} = (\delta_\Delta/\delta_{c,m})^{\beta_{res}}$, Eq. (36) becomes:

$$\frac{1}{\Xi_{res}}\frac{d\Xi_{res}}{dt^+} = \alpha Ka \ln\left(\frac{l_t}{\delta_\Delta}\right) - \gamma\left(\frac{\delta_c}{\delta_{c,m}}\right)^{\beta_{res}} \ln\left(\Xi_{res}\right) \qquad (43)$$

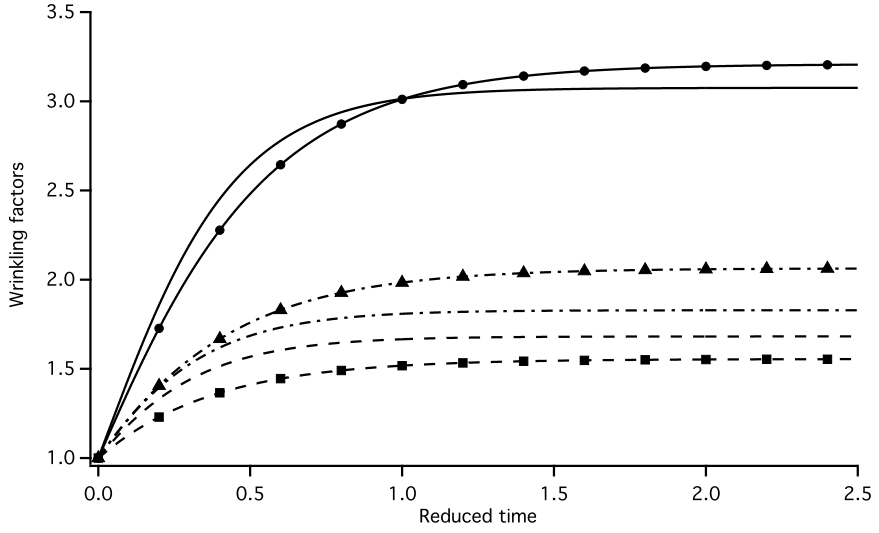

Figure 8: Evolution of the total (Ξ_{tot}, continuous line), resolved (Ξ_{res}, dotted-dashed line) and sub-grid scale (Ξ_{sgs}, dashed line) surface wrinkling factors as a function of the reduced time $t^+ = t/\tau_f$. Without markers: exact fractal reference solution; with markers: solution given by Eq. (36) combined with the dynamic model setting $\delta_{c,m} = 1.5\delta_c$.

Figure 8 displays the time evolution of the various flame surfaces for $\delta_{c,m} = 1.5\delta_c$. As expected, the strong overestimation of the sub-grid scale flame surface at early stages when using a constant value of Ξ_{sgs} is no longer observed, in agreement with practical implementation of the dynamic model [37, 38]: by construction, $\Xi_{sgs}(t^+ = 0) = 1$. The underestimation of the

sub-grid scale surface due to the overestimated flame cut-off length scale is largely compensated by the larger resolved flame surface (overestimation of the total flame surface at equilibrium of about 4 %, to be compared to 20 % in Fig. 6).

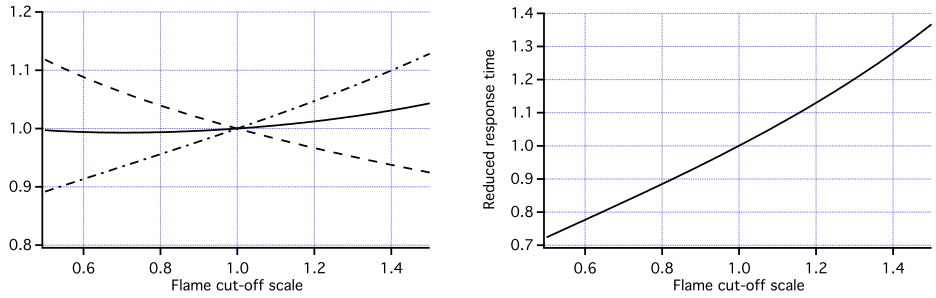

Figure 9: Evolution as a function of the flame cut-off length scale $\delta_{c,m}/\delta_c$ of equilibrium values of total (Ξ_{tot}, continuous line), resolved (Ξ_{res}, dotted-dashed line) and sub-grid scale (Ξ_{sgs}, dashed line) surface wrinkling factors reduced by their exact values (left) and of the flame response time τ_w reduced by its exact value (right) using the dynamic formalism.

Figure 9 shows that the over- or under-estimation of the sub-grid scale surface when varying the prescribed inner cut-off scale $\delta_{c,m}$ is almost perfectly compensated by the under- or over-estimation of the resolved flame surface, respectively, significantly reducing errors on the overall flame surface and turbulent flame speed at the equilibrium. The temporal evolution of the flame is also affected by the set inner cut-off scale value but to a far lesser extent than when using the constant wrinkling factor model (compare Figs 7 and 9) while the correct flame response is recovered with the exact inner cut-off scale. This finding might explain why Volpiani et al. [41] correctly predicted an unstable mode of a turbulent swirling flame with a dynamic

model while a non-dynamic formulation failed.

5. Conclusion

A framework is proposed to investigate the behavior of LES flame surface density models for simple academic cases, here the development of a statistically one-dimensional flame in an homogenous and isotropic turbulence, by comparison with a prescribed reference solution. The first step is to derive the corresponding set of balance equations, here to reproduce a fractal flame surface with a fractal dimension evolving with time from a initially planar flame up to equilibrium. Then, a balance equation is solved to mimic the evolution of the resolved flame surface in an actual large eddy simulation. Non-dynamic and dynamic versions of an unresolved surface wrinkling factor model are investigated including the influence of model parameters, the fractal dimension of the unresolved surface for the non-dynamic model, estimated from resolved scale in the dynamic approach, and the inner cut-off flame length scale for both formalisms. The non-dynamic formulation overestimates the total flame surface in early stage of the flame development, as already observed in the literature [35, 37, 38], while an overestimation of the sub-grid scale flame surface is partly compensated by a lower resolved flame surface and vice-versa. As expected, the dynamic formulation is found to better reproduce the reference solution. However, models and parameters are found to influence the flame response time, but in a lower extent with the dynamic formulation, possibly affecting the prediction of combustion instabilities [41].

Of course, the generality of conclusions are clearly limited by the choice

of the enforced reference solution and the corresponding balance equation closures but we feel this approach is well-suited to quickly exploring with negligible computational costs the qualitative behavior of sub-grid scale models, to support the design of direct numerical simulations, as well as to help in analyzing large eddy simulations results or perform uncertainty quantifications. Moreover, this analysis suggests unusual scalings for strain rate (Eq. 20) or curvature (Eqs 31 and 34) terms, written as logarithm of the length scale and the flame surface wrinkling factor, respectively, or relating the mean flame surface wrinkling length scale to the flame inner cut-off scale. The derivation also identifies a contribution of resolved length scales to the sub-grid flame surface wrinkling factor (Eq. 39). The relevance of these formulations has now to be investigated.

The formulation proposed here is a first step to be refined. First, some closures have to be revisited. The assumption of a fractal structure of the flame surface at each stage of its development (i.e. the flame is wrinkled simultaneously at all scales ranging from the inner cut-off to the turbulence integral length scales) as well as the rather ad hoc closure for the resolved surface curvature (Eq. 34) are questionable. The expected bending of the fractal dimension when increasing the Karlovitz number Ka is also not predicted. We identified the inner cut-off scales of the total (δ_c) and resolved (δ_Δ) flame surfaces to the laminar flame thickness δ_L and the filter size Δ, respectively but they could differ (Colin et al. [21] suggested a reduced ability of turbulent motions smaller that 5Δ to wrinkle the resolved flame surface). In the dynamic formalism, the model exponent β is estimated here from the overall resolved flame surface without mimicking the actual test-filtering

operation, with a test filter width only slightly larger than the filter size Δ. Another configuration of interest regarding combustion instabilities would be to study the flame response predicted by models, in terms of amplification or damping and phase shift, to periodic flow perturbations. All these points will be investigated in a near future.

Acknowledgments

Kenneth Bray's pioneering and outstanding contributions to combustion researches have largely and deeply inspired thinking and works of the author who, beyond that, would like also to warmly thank him for the very fruitful exchanges from which he benefited, in particular regarding the analysis of the phenomena of turbulent transport gradient and counter-gradient in turbulent premixed flames.

AppendixA. Strain rate modeling according to Charlette et al.

Considering homogeneous and isotropic turbulence, Charlette et al. [23] modeled the strain rate acting on the flame surface and due to turbulent motions up to the integral length scale l_t as:

$$\langle a \rangle_{tot}^2 = \int_{\pi/l_t}^{+\infty} \left[C\left(k\right) \right]^2 k^2 E_{11}\left(k\right)\, dk \tag{A.1}$$

where $E_{11}(k)$ is the one-dimensional (longitudinal) energy spectrum in the direction of the wavenumber k and $C(k)$ an efficiency function taking into account the ability of the turbulent eddy at scale π/k to stretch the flame. Using the standard longitudinal Kolmogorov spectrum including the Pao

correction for viscous cut-off:

$$E_{11}(k) = \frac{18}{55} C_k \varepsilon^{2/3} k^{-5/3} \exp\left(-\frac{3}{2} C_k (k\eta)^{4/3}\right) \tag{A.2}$$

where ε is the turbulence dissipation rate, η the Kolmogorov length scale and $C_k \approx 1.5$ the universal Kolmogov constant, and assuming the flame behaves as a low pass filter in the wavenumber space k:

$$C(k) = 1 \quad \text{when} \quad k \leq \frac{\pi}{\delta_c} \quad ; \quad C(k) = 0 \quad \text{elsewhere} \tag{A.3}$$

i.e. only turbulent motions larger than the flame inner cut-off scale δ_c effectively stretch the flame front, Eq. (A.1) gives the analytical expression:

$$\langle a \rangle_{tot} = \frac{3}{\sqrt{55}} Ka \frac{S_L}{\delta_L} \left[\exp\left(-\frac{3}{2} C_k \frac{\pi^{4/3}}{Re_t}\right) - \exp\left(-\frac{3}{2} C_k \frac{\pi^{4/3}}{Re_t} \left(\frac{l_t}{\delta_c}\right)^{4/3}\right) \right]^{1/2} \tag{A.4}$$

using usual relations for homogenous and isotropic turbulence ($\varepsilon = u'^3/l_t$, $\eta = (\nu^3/\varepsilon)^{1/4}$, where u' is the velocity fluctuation related to integral length scale l_t and ν the kinematic viscosity) and premixed flame ($S_L \delta_L / \nu \approx 1$). $Re_t = u' l_t / \nu$ is the turbulence Reynolds number and $Ka = (u'/S_L)^{3/2} (l_t/\delta_L)^{-1/2}$ the Karlovitz number [27]. Note that $(1/Re_t)(l_t/\delta_c)^{4/3} = 1/Re_c$ where Re_c is the Reynolds number corresponding to the cut-off scale δ_c. In the limit $\delta_c \to 0$ and large turbulence Reynolds numbers, Eq. (A.4) reduces to:

$$\langle a \rangle_{tot} = \frac{3}{\sqrt{55}} Ka \frac{S_L}{\delta_L} = \frac{3}{\sqrt{55}} \sqrt{\frac{\varepsilon}{\nu}} \tag{A.5}$$

proportional to the inverse of a Kolmogorov time scale, as suggested by Cant et al. [12].

Equation (A.1) provides an order of magnitude only. It assumes a cumulative effect of independent turbulent motions, neglecting possible interactions

and their effects on flame surface and, as based on energy, cannot recover the expected relation $\langle a \rangle_{tot} = \langle a \rangle_{sgs} + \langle a \rangle_{res}$ with $\langle a \rangle_{sgs}$ and $\langle a \rangle_{res}$ computed within the range of turbulent scales $[\delta_c, \delta_\Delta]$ and $[\delta_\Delta, l_t]$, respectively, predicting instead $\langle a \rangle_{tot}^2 = \langle a \rangle_{sgs}^2 + \langle a \rangle_{res}^2$. Kolla et al. [2014, 2016] evidenced that the turbulent kinetic energy spectrum for turbulent premixed flames could differ from that of constant density non-reacting flows (here, Eq. A.2). However, these differences induced by heat release are observed for scales of the order or smaller than the laminar flame thickness, having low efficiency values and ruled out here by the Heaviside function (A.3). Despite of these strong assumptions, the ITNFS model [43] for RANS as well as the LES efficiency functions derived following this approach [21, 23, 78] were widely and successfully used in practical simulations.

References

[1] K. Bray, P. Libby, Interaction effects in turbulent premixed flames, Phys. Fluids 19 (1976) 1687–1701.

[2] K. Bray, J. Moss, A unified statistical model of the premixed turbulent flame, Acta Astronautica 4 (1977) 291 – 319.

[3] P. Libby, K. Bray, J. Moss, Effects of finite reaction rate and molecular transport in premixed turbulent combustion, Combust. Flame 34 (1979) 285–301.

[4] K. Bray, Turbulent flows with premixed reactants, in: P. Libby, F. Williams (Eds.), Turbulent Reacting Flows, Springer, 1980.

[5] P. A. Libby, K. Bray, Implications of the laminar flamelet model in premixed turbulent combustion, Combust. Flame 39 (1980) 33–41.

[6] K. Bray, P. Libby, G. Masuya, J. Moss, Turbulence production in premixed turbulent flames, Combustion Science and Technology 25 (1981) pp 127 – 140.

[7] K. Bray, J. Moss, P. Libby, Turbulent transport in premixed turbulent flames, in: J. Zierep, H. Oertel (Eds.), Convective Transport and Instability Phenomena, University of Karlsuhe, Germany, 1982.

[8] K. Bray, M. Champion, P. Libby, The interaction between turbulence and chemistry in premixed turbulent flames, in: R. Borghi, S. Murphy (Eds.), Turbulent Reacting Flows, volume 40 of *Lecture Notes in Engineering*, Springer, 1989, pp. 541 – 563.

[9] S. Pope, The evolution of surfaces in turbulence, Int. J. Engineering Science 26 (1988) 445–469.

[10] S. Candel, D. Veynante, F. Lacas, E. Maistret, N. Darabiha, T. Poinsot, Coherent flame model : applications and recent extensions, in: B. E. Larrouturou (Ed.), Advances in combustion modeling. Series on advances in mathematics for applied sciences, World Scientific, Singapore, 1990, pp. 19–64.

[11] S. Candel, T. Poinsot, Flame stretch and the balance equation for the flame area, Combust. Sci. Technol. 70 (1990) 1–15.

[12] R. Cant, S. Pope, K. Bray, Modelling of flamelet surface to volume ratio

in turbulent premixed combustion, Symp. (Int.) Combust. 23 (1990) 809–815.

[13] H. G. Weller, C. J. Marooney, A. D. Gosman, A new spectral method for calculation of the time-varying area of a laminar flame in homogeneous turbulence, Symp. (Int.) Combust. 23 (1991).

[14] J. Duclos, D. Veynante, T. Poinsot, A comparison of flamelet models for premixed turbulent combustion, Combust. Flame 95 (1993) 101–118.

[15] A. Trouvé, T. Poinsot, The evolution equation for the flame surface density., J. Fluid Mech. 278 (1994) 1–31.

[16] L. Vervisch, E. Bidaux, K. Bray, W. Kollmann, Surface density function in premixed turbulent combustion modeling, similarities between probability density function and flame surface approach, Phys. Fluids 7 (1995) 2496 – 2503.

[17] F. Marble, J. Broadwell, The coherent flame model for turbulent chemical reactions., Technical Report TRW-9-PU, Project Squid, 1977.

[18] M. Boger, D. Veynante, H. Boughanem, A. Trouvé, Direct numerical simulation analysis of flame surface density concept for large eddy simulation of turbulent premixed combustion, Symp. (Int.) Combust. 27 (1998) 917 – 925.

[19] H. Weller, G. Tabor, A. Gosman, C. Fureby, Application of a flame-wrinkling LES combustion model to a turbulent mixing layer, Symp. (Int.) Combust. 27 (1998) 899 – 907.

[20] C. Nottin, R. Knikker, M. Boger, D. Veynante, Large eddy simulations of an acoustically excited turbulent premixed flame, Proc. Combust. Inst. 28 (2000) 67 – 73.

[21] O. Colin, F. Ducros, D. Veynante, T. Poinsot, A thickened flame model for large eddy simulations of turbulent premixed combustion, Phys. Fluids A 12 (2000) 1843 – 1863.

[22] E. Hawkes, S. Cant, A flame surface density approach to large eddy simulation of premixed turbulent combustion, Proc. Combust. Inst. 28 (2000) 51 – 58.

[23] F. Charlette, C. Meneveau, D. Veynante, A power-law flame wrinkling model for LES of premixed turbulent combustion. Part I: Non-dynamic formulation and initial tests, Combust. Flame 131 (2002) 159 – 180.

[24] D. Veynante, L. Vervisch, Turbulent combustion modeling, Prog. Energy Combust. Sci. 28 (2002) 193 – 266.

[25] S. Richard, O. Colin, O. Vermorel, A. Benkenida, C. Angelberger, D. Veynante, Towards large eddy simulation of combustion in spark ignition engines, Proc. Combust. Inst. 31 (2007) 3059 – 3066.

[26] S. R. Gubba, S. S. Ibrahim, W. Malalasekera, A. R. Masri, An assessment of large eddy simulations of premixed flames propagating past repeated obstacles, Combust. Theory and Modelling 13 (2009) 513–540.

[27] T. Poinsot, D. Veynante, Theoretical and Numerical Combustion, http://elearning.cerfacs.fr/combustion, 3rd edition, 2011.

[28] R. Knikker, D. Veynante, C. Meneveau, A priori testing of a similarity model for large eddy simulations of turbulent premixed combustion, Proc. Combust. Inst. 29 (2002) 2105 – 2111.

[29] S. Gubba, S. Ibrahim, W. Malalasekera, A. Masri, Measurements and les calculations of turbulent premixed flame propagation past repeated obstacles, Combust. Flame 158 (2011) 2465 – 2481.

[30] S. R. Gubba, S. S. Ibrahim, W. Malalasekera, Dynamic flame surface density modelling of flame deflagration in vented explosion, Combustion, Explosion and Shock Waves 48 (2012) 393–405.

[31] F. Charlette, C. Meneveau, D. Veynante, A power-law flame wrinkling model for LES of premixed turbulent combustion. Part II: Dynamic formulation, Combust. Flame 131 (2002) 181 – 197.

[32] R. Knikker, D. Veynante, C. Meneveau, A dynamic flame surface density model for large eddy simulation of turbulent premixed combustion, Phys. Fluids 16 (2004) L91 – L94.

[33] S. Ibrahim, S. Gubba, A. Masri, W. Malalasekera, Calculations of explosion deflagrating flames using a dynamic flame surface density model, Journal of Loss Prevention in the Process Industries 22 (2009) 258 – 264.

[34] G. Wang, M. Boileau, D. Veynante, Implementation of a dynamic thickened flame model for large eddy simulations of turbulent premixed combustion, Combust. Flame 158 (2011) 2199–2213.

[35] G. Wang, M. Boileau, D. Veynante, K. Truffin, Large eddy simulation of a growing turbulent premixed flame kernel using a dynamic flame surface density model, Combust. Flame 159 (2012) 2742 – 2754.

[36] T. Schmitt, A. Sadiki, B. Fiorina, D. Veynante, Impact of dynamic wrinkling model on the prediction accuracy using the F-TACLES combustion model in swirling premixed turbulent flames, Proc. Combust. Inst. 34 (2013) 1261–1268.

[37] D. Veynante, V. Moureau, Analysis of dynamic models for large eddy simulations of turbulent premixed combustion, Combust. Flame 162 (2015) 4622 – 4642.

[38] T. Schmitt, M. Boileau, D. Veynante, Flame wrinkling factor dynamic modeling for large eddy simulations of turbulent premixed combustion, Flow Turb. Combust. 94 (2015) 199–217.

[39] A. Hosseinzadeh, A. Sadiki, J. Janicka, Assessment of the dynamic SGS wrinkling combustion modeling using the thickened flame approach coupled with FGM tabulated detailed chemistry, Flow Turb. Combust. (2016) 1–26.

[40] P. Volpiani, T. Schmitt, D. Veynante, A posteriori tests of a dynamic thickened flame model for large eddy simulations of turbulent premixed combustion, Combust. Flame 174 (2016) 166 – 178.

[41] P. Volpiani, T. Schmitt, D. Veynante, Large eddy simulation of a turbulent swirling premixed flame coupling the TFLES model with a dynamic wrinkling formulation, Combust. Flame 180 (2017) 124 – 135.

[42] P. Volpiani, T. Schmitt, O. Vermorel, P. Quillatre, D. Veynante, Large eddy simulation of explosion deflagrating flames using a dynamic wrinkling formulation, Combust. Flame 186 (2017) 17 – 31.

[43] C. Meneveau, T. Poinsot, Stretching and quenching of flamelets in premixed turbulent combustion, Combust. Flame 86 (1991) 311–332.

[44] O. Colin, M. Rudgyard, Development of high-order Taylor-Galerkin schemes for LES, J. Comput. Phys. 162 (2000) 338 – 371.

[45] N. Chakraborty, M. Klein, A priori direct numerical simulation assessment of algebraic flame surface density models for turbulent premixed flames in the context of large eddy simulation, Phys. Fluids 20 (2008).

[46] N. Chakraborty, R. S. Cant, Direct Numerical Simulation analysis of the Flame Surface Density transport equation in the context of Large Eddy Simulation, Proc. Combust. Inst. 32 (2009) 1445–1453.

[47] N. Chakraborty, R. S. Cant, Effects of Lewis number on flame surface density transport in turbulent premixed combustion, Combust. Flame 158 (2011) 1768–1787.

[48] M. Katragadda, S. P. Malkeson, N. Chakraborty, Modelling of the tangential strain rate term of the Flame Surface Density transport equation in the context of Reynold Averaged Navier-Stokes simulation, Proc. Combust. Inst. 33 (2011) 1429–1437.

[49] E. Hawkes, O. Chatakonda, H. Kolla, A. Kerstein, J. Chen, A petascale direct numerical simulation study of the modelling of flame wrinkling

for large-eddy simulations in intense turbulence, Combust. Flame 159 (2012) 2690 – 2703.

[50] S. P. Malkeson, N. Chakraborty, Statistical Analysis and a-priori Modelling of Flame Surface Density Transport in Turbulent Stratified Flames: A Direct Numerical Simulation Study, Flow Turb. Combust. 90 (2012) 143–187.

[51] N. Chakraborty, R. S. Cant, Turbulent Reynolds number dependence of flame surface density transport in the context of Reynolds averaged Navier-Stokes simulations, Proc. Combust. Inst. 34 (2013) 1347–1356.

[52] M. Katragadda, S. P. Malkeson, N. Chakraborty, Modelling of the curvature term in the flame surface density transport equation: A direct numerical simulations based analysis, Int. J. Spray and Comb. Dynamics 6 (2014) 163–198.

[53] T. Ma, O. Stein, N. Chakraborty, A. Kempf, A posteriori testing of the flame surface density transport equation for LES, Combust. Theory and Modelling 18 (2014) 32–64.

[54] F. Gouldin, An application of fractals to modeling premixed turbulent flames, Combust. Flame 68 (1987) 249 – 266.

[55] F. Gouldin, K. Bray, J.-Y. Chen, Chemical closure model for fractal flamelets, Combust. Flame 77 (1989) 241 – 259.

[56] F. Gouldin, S. Hilton, L. T., Experimental evaluation of the fractal geometry of flamelets, Symp. (Int.) Combust. 22 (1989) 541 – 550.

[57] G. North, D. Santavicca, The fractal nature of premixed turbulent flames, Combust. Sci. Technol. 72 (1990) 215–232.

[58] O. Gulder, Turbulent premixed combustion modelling using fractal geometry, Symp. (Int.) Combust. 23 (1991) 835–842.

[59] N. Peters, Turbulent combustion, Cambridge University Press, 2000.

[60] E. Giacomazzi, C. Bruno, B. Favini, Fractal modelling of turbulent combustion, Combust. Theory and Modelling 4 (2000) 391–412.

[61] E. Giacomazzi, V. Battaglia, C. Bruno, The coupling of turbulence and chemistry in a premixed bluff-body flame as studied by LES, Combust. Flame 138 (2004) 320 – 335.

[62] N. Aluri, S. Muppala, F. Dinkelacker, Substantiating a fractal-based algebraic reaction closure of premixed turbulent combustion for high pressure and the lewis number effects, Combust. Flame 145 (2006) 663–674.

[63] E. Giacomazzi, F. R. Picchia, N. Arcidiacono, D. Cecere, F. Donato, B. Favini, Unsteady simulation of a CO/H2/N2/air turbulent non-premixed flame, Combust. Theory and Modelling 12 (2008) 1125–1152.

[64] F. Cavallo Marincola, T. Ma, A. Kempf, Large eddy simulations of the darmstadt turbulent stratified flame series, Proc. Combust. Inst. 34 (2013) 1307–1315.

[65] R. Keppeler, E. Tangermann, U. Allaudin, M. Pfitzner, LES of Low

to High Turbulent Combustion in an Elevated Pressure Environment, Flow Turb. Combust. 92 (2014) 767–802.

[66] G. Kuenne, A. Ketelheun, J. Janicka, Les modeling of premixed combustion using a thickened flame approach coupled with fgm tabulated chemistry, Combust. Flame 158 (2011) 1750–1767.

[67] B. Fiorina, R. Vicquelin, P. Auzillon, N. Darabiha, O. Gicquel, D. Veynante, A filtered tabulated chemistry model for LES of premixed combustion, Combust. Flame 157 (2010) 465–475.

[68] S. Bougrine, S. Richard, O. Colin, D. Veynante, Fuel Composition Effects on Flame Stretch in Turbulent Premixed Combustion: Numerical Analysis of Flame-Vortex Interaction and Formulation of a New Efficiency Function, Flow Turb. Combust. 93 (2014) 259–281.

[69] F. Thiesset, G. Maurice, F. Halter, N. Mazellier, C. Chauveau, I. Gokalp, Flame-vortex interaction: Effect of residence time and formulation of a new efficiency function, Proc. Combust. Inst. 36 (2017) 1843 – 1851.

[70] O. Gulder, G. Smallwood, Inner cutoff scale of flame surface wrinkling in turbulent premixed flame, Combust. Flame 103 (1995) 107 – 114.

[71] N. Peters, P. Terhoeven, J. Chen, T. Echekki, Statistics of flame displacement speeds from computations of 2-d unsteady methane-air flames, Symp. (Int.) Combust. 27 (1998) 833 – 839.

[72] C. J. Rutland, T. A., Direct simulations of premixed turbulent flames with nonunity Lewis numbers, Combust. Flame 94 (1993) 41–57.

[73] R. Lindstedt, E. Vaos, Modeling of premixed turbulent flames with second moment methods, Combust. Flame 116 (1999) 461 – 485.

[74] B. Renou, A. Boukhalfa, D. Puechberty, M. Trinité, Local scalar flame properties of freely propagating premixed turbulent flames at various Lewis numbers, Combust. Flame 123 (2000) 507–521.

[75] S. Richard, D. Veynante, A 0-D flame wrinkling equation to describe the turbulent flame surface evolution in SI engines, Comptes Rendus de Mécanique 343 (2015) 219–231.

[76] H. Kolla, E. R. Hawkes, A. Kerstein, N. Swaminathan, J. Chen, On velocity and reactive scalar spectra in turbulent premixed flames, J. Fluid Mech. 754 (2014) 456–487.

[77] H. Kolla, X.-Y. Zhao, J. Chen, N. Swaminathan, Velocity and reactive scalar dissipation spectra in turbulent premixed flames, Combustion Science and Technology 188 (2016) 1424–1439.

[78] S. Bougrine, S. Richard, J. Michel, D. Veynante, Simulation of CO and NO emissions in a si engine using a 0D coherent flame model coupled with a tabulated chemistry approach, Applied Energy 113 (2014) 1199 – 1215.